ACS APPLIED MATERIALS & INTERFACES

Research Article

www.acsami.org

Preparation of Vertically Oriented TiO_2 Nanosheets Modified Carbon Paper Electrode and Its Enhancement to the Performance of MFCs

Tao Yin,[†] Zhenya Lin,[†] Lin Su,[†] Chunwei Yuan,[†] and Degang Fu*[,†,‡,§]

[†]State Key Laboratory of Bioelectronics, Southeast University, Nanjing 210096, People's Republic of China

[‡]Suzhou Key Laboratory of Environment and Biosafety, Suzhou 215123, People's Republic of China

[§]Jiangsu Key Laboratory for Biomaterials and Devices, Southeast University, Nanjing 210096, People's Republic of China

Supporting Information

ABSTRACT: A unique vertically oriented TiO_2 nanosheets (TiO_2-NSs) layer was synthesized in situ on the surface of a carbon paper (CP) electrode via hydrothermal synthesis upon addition of a suitable amount of activated carbon powders in a reactor. Field emission scanning electron microscopy images showed that the nanosheets were about 2 μm in length, 200−600 nm in width and 15 nm in thickness. X-ray diffraction and Raman patterns verified TiO_2-NSs crystallized in the anatase phase. The electrochemical activities of CP and TiO_2-NSs/CP electrode have been investigated by cyclic voltammetry and electrochemical impedance spectroscopy. The maximum power output density of a mixed consortia inoculated microbial fuel cell was increased by 63% upon using TiO_2-NSs/CP as a bioanode compared with that using bare CP as a bioanode. The performance improvement could be ascribed to unique 3D open porous interface made of vertically oriented TiO_2-NSs, which provides good biocompatibility, favorable mass transport process, large surface areas for adhesion of bacteria and direct pathways for electron movement to the electrode.

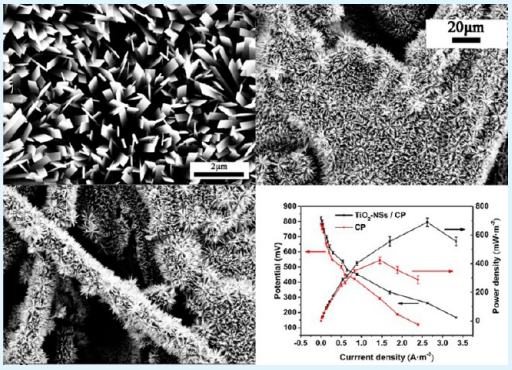

KEYWORDS: *TiO_2 nanosheets, extracellular electron transfer, MFCs, bioelectronics, carbon electrode*

INTRODUCTION

In a microbial fuel cell (MFC), microbial metabolism can directly convert chemical energy in organic compounds to electricity by the way of extracellular electron transfer (EET), which can proceed through direct physical contact of bacterial cells with the anode via outer membrane c-type cytochromes (OMCs), pilus or indirectly by soluble electron mediators, such as self-secreted flavins.[1−3] To improve the performance of MFCs, several strategies have been applied to enhance the bacterial EET. One promising technology is genetic the engineering approach as illustrated by some excellent research, e.g., enhancing membrane permeability of *Escherichia coli* via expressing a porin protein OprF with the gene from *P. aeruginosa* PAO1,[4] overexpressing quorum sensing system in *Pseudomonas aeruginosa*,[5] displaying O_2-reducing enzymes on the surface of *Saccharomyces cerevisiae*.[6] Another effective strategy is designing and fabricating a high performance electrode, as the electrode provides surface active sites for microbial adhesion and interfacial electron transfer. At present, anodes of MFCs are often made of carbon based materials, such as graphite fiber brush, carbon paper, reticulated vitreous carbon, carbon nanofibers, etc.,[7] mainly due to their good biocompatibility, electrical conductivity and chemical stability as well as low cost,[8,9] and various chemical and physical approaches for anode modification have been employed to favor the formation of biofilm and the direct electron exchange between bacteria and the anode.[7,10] Nanomaterials including conductive polymer, graphene, carbon nanotubes (CNTs) and semiconductors are often used to construct a rough surface with high anodic "bioaccessible" surface area and conductivity.[7]

Metal oxide semiconductors with plenty of tailored nanostructures have been extensively investigated for the development of electrochemical biosensors,[11] electronic devices[12] and energy transducers,[13] and also have been used to modify anodes in MFCs.[14] For example, iron oxides are well-known semiconductor materials that can act as terminal electron acceptors for dissimilatory metal-reducing bacterium, such as *Shewanella oneidensis* commonly found in near-surface earth environments,[15] and also can promote a long-distance EET processes in the bacterial networks[16] as well as improve the performance of a bioanode.[17] It is interesting to note that some metal oxides (rutile, goethite) can not only enhance the EET in MFCs but also stimulate the growth of chemo-autotrophic and heterotrophic bacteria using solar energy.[18]

TiO_2 is one of the most attractive metal oxides used in many areas concerning solar cells,[19] photocatalysis,[20] sensors,[21] supercapacitor,[22] etc. TiO_2 has very good chemical stability and biocompatibility, and also is abundant and environment-

Received: September 17, 2014
Accepted: December 4, 2014
Published: December 4, 2014

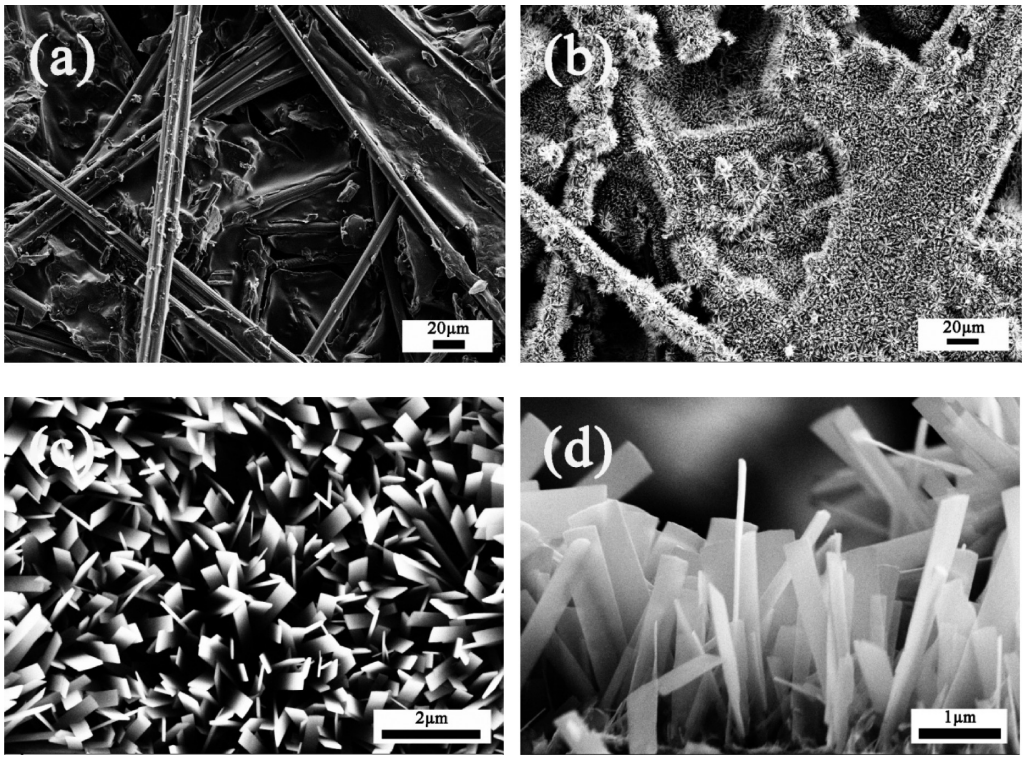

Figure 1. FESEM images of the bare CP electrode (a), TiO_2-NSs/CP electrode (b, c) and its cross section (d). TiO_2-NSs/CP electrode obtained under optimal conditions.

friendly.[23] These advantages are very attractive for practical MFC electrodes. Qiao et al. reported that mesoporous TiO_2 with a flake-cross-linked structure composited with 30 wt % polyaniline (PANI) as the MFC anode gave the best bio- and electrocatalytic performance.[24] It is postulated that the mesoporous TiO_2 provides high specific surface area and good biocompatibility, which is suitable for the growth of *E. coli* as well as the mass transfer. Wen et al. obtained a modified carbon cloth anode for MFCs by deposition of the nanohybrids of anatase TiO_2 nanoparticles-decorated CNTs (CNTs@TiO_2).[25] This modification significantly improved the power density compared with the modification by pure TiO_2 nanoparticles or CNTs alone. TiO_2 nanoparticle modified electrode exhibited a slightly smaller output current I_{max} than that of CNTs modified electrode (3.25 vs 3.64 A cm^{-2}), one of the reasons may be large resistance of TiO_2 nanoparticle film due to the electron transport obstruction at grain boundaries. However, the electron transport in semiconductor nanomaterial/nanostructures could be improved after different kinds of optimization.[26−28] For instance, the charge transfer was enhanced in the film of TiO_2 hierarchical microspheres (HMSs) assembled by nanospindles than in the film composed of nanoparticles due to improved interparticle connection.[29] In fact, one-dimensional TiO_2 nanostructures with a relatively small amount of grain boundaries which are able to provide fast electron transport have been extensively used in photoanodes for efficient dye sensitized solar cells (DSSCs).[30] We expect that an oriented TiO_2 nanostructure on an anode of a MFC may promote EET of exoelectrogens.

Herein, we reported the fabrication of vertically oriented TiO_2 nanosheets (NSs) on the surface of carbon paper (CP) electrode. The modified electrode, denoted as TiO_2-NSs/CP, was used as the anode of the MFC inoculated with sludge from the wastewater treatment plant. The morphology, structure, electrochemical activity of the electrode and the power output of the MFC were investigated. It was found that the maximum power density of the MFC equipped with TiO_2-NSs/CP anode has been distinctly improved. The results highlighted the potential of suitably tailored nanostructures made of metal oxide semiconductors for optimizing the performance of an anode as well as MFCs. To the best of our knowledge, this is a first case reported that oriented TiO_2 nanostructure was applied in the anode of MFCs to facilitate EET of bacteria without compositing other conductive materials.

EXPERIMENTAL SECTION

Materials and Reagents. Carbon paper was purchased from ShangHai HESEN Electrical Appliance Co. Ltd. Activated carbon (AC) powder was purchased from Nanjing Chemical Reagent Co., Ltd. Proton exchange membrane (PEM, Nafion 117) was from DuPont (Wilmington, DE). Tetrabutyl titanate was purchased from ChengDu KeLong Chemical Co., Ltd. All reagents were of analytical grade and the solvent was ultrapure water. Before use, CP was ultrasonically cleaned for 60 min with acetone, ethanol and distilled water respectively, then dried in an oven at 80 °C.

Preparation of TiO_2 Nanosheets Modified CP Electrode (TiO_2-NSs/CP). TiO_2 sol was synthesized in a laboratory following a previous report.[31] The clean CP was immersed into the TiO_2 sol for 10 min and dried at 80 °C. After that, it was calcined for 30 min in a tubular furnace at 350 °C to forming a TiO_2 seed layer on the CPs' surface. The Teflon-lined stainless steel autoclave (50 mL in volume) filled with 40 mL of aqueous solution of 10 M NaOH and 0.2 g of AC powders was placed in an oven at 180 °C for 24 h. After the CP cooled down to room temperature, the modified CP was rinsed with ultrapure water to remove AC, followed by soaking with 0.1 M hydrochloric acid for 1 h, then washed to neutral with deionized water and dried at 80 °C. Sequentially, the sample was calcined at 550 °C for 1 h in a N_2 atmosphere.

MFC Setup and Operation. A dual-chamber MFC (each chamber with a volume of 330 mL and sealed with rubber stoppers) was

dx.doi.org/10.1021/am506360x | ACS Appl. Mater. Interfaces 2015, 7, 400−408

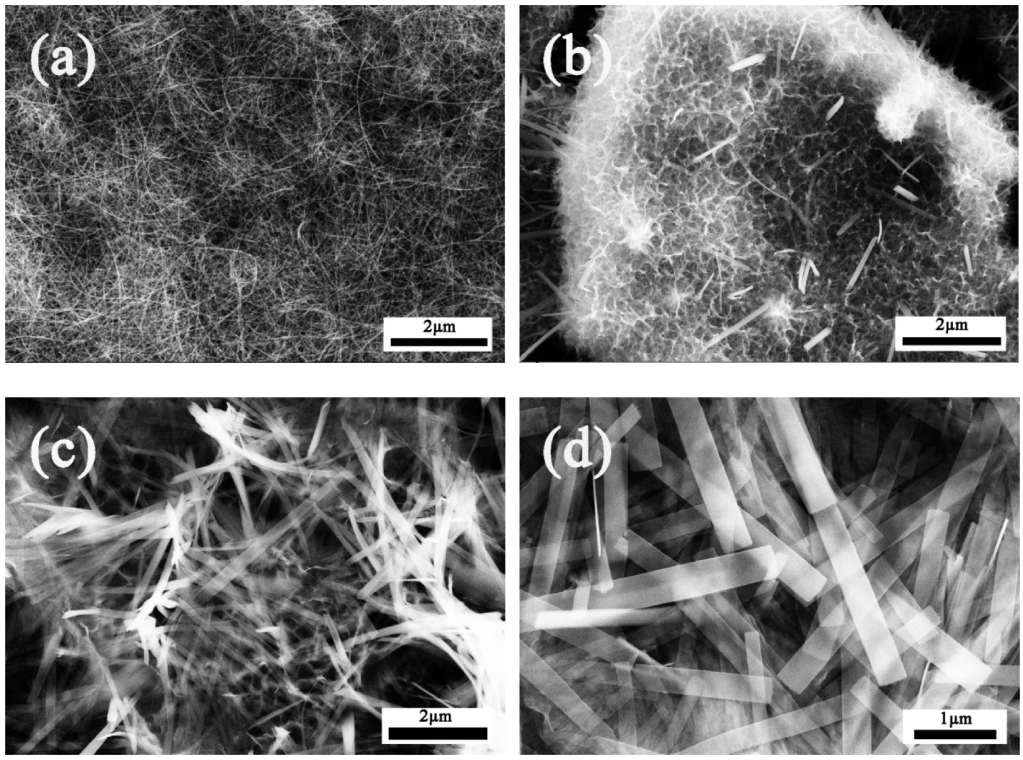

Figure 2. FESEM images of modified CP electrodes obtained under 0 mg (a), 50 mg (b), 150 mg(c) and 250 mg (d) of AC powders in a hydrothermal reactor.

constructed with two bottles separated by PEM with a projected area of 9.6 cm^2. TiO_2-NSs/CP (2 × 2.5 cm) and bare CP (3 × 3 cm) were used as the anode and cathode, respectively, with an electrode spacing of 8 cm.

The anode compartment was initially inoculated with a mixture of anaerobic sludge obtained from Wastewater Treatment Plant of Nanjing City and the cultivation medium (1:3, V/V). The cultivation medium (pH = 7) contained (per liter): 4.4 g of KH_2PO_4, 3.4 g of $K_2HPO_4{\cdot}3H_2O$, 1.6 g of CH_3COONa, 1.5 g of NH_4Cl, 0.1 g of $MgCl_2{\cdot}6H_2O$, 0.1 g of $CaCl_2{\cdot}2H_2O$, 0.1 g of KCl and 10 mL of trace mineral metals solution.[32] The anolyte contained 300 mL cultivation medium, whereas the 300 mL catholyte contained 50 mM potassium ferricyanide ($K_3[Fe(CN)_6]$) and 100 mM PBS (phosphate buffer solution). At the start-up stage, the anode and cathode connected to a 1 kΩ resistor using copper wire and nonconductive epoxy resin was utilized for isolating exposed metal surfaces from solutions. After the output voltage was stable for two consecutive cycles, the cell was ready for measuring polarization and power output curves. The measurement was done by varying the external resistor over a range from 30 to 50 Ω and then monitored the MFC steady-state voltage. All the experiments were operated at 30 ± 0.5 °C in anaerobic conditions.

The control experiment was performed in same conditions except using bare CP (2 × 2.5 cm) as the anode.

Characterization and Measurement. The surface morphology was observed by a field emission scanning electron microscopy (FESEM) with a Zeiss Ultra Plus (Zeiss, Germany) instrument. The crystalline structure was characterized by X-ray diffraction (XRD) recorded by an XD-3A (Shimadzu Corporation, Japan) instrument using graphite monochromatic copper radiation (Cu Kα) at 40 kV and 30 mA over the 2θ range of 10−80°. Raman spectra were measured under the 785 nm excitation wavelength using an inVia Raman Microscope (Renishaw Corporation, United Kingdom).

Electrochemical measurements were carried out by CHI760d electrochemical workstation (CH Instruments Inc., China) with the three-electrode system, but electrochemical impedance spectroscopy (EIS) measurements were conducted using an IM6ex electrochemical workstation (Zahner, Germany) with the voltage amplitude of 5 mV over the frequency range from 100 kHz to 0.01 Hz. The cyclic voltammogram (CV) and EIS measurements in an electrolyte solution consisting of 50 mM $K_3[Fe(CN)_6]$ and 100 mM PBS were performed using a single-chamber electrochemical reactor described elsewhere.[16] CP or TiO_2-NSs/CP placed on the bottom of the reactor was used as the working electrode, with Pt wire and a saturated calomel electrode (SCE) as the counter and reference electrodes, respectively. When electrochemical measurements were performed in the MFCs, the anode and cathode acted as the working electrode and counter electrode, respectively, with SCE inserted into the anolyte as a reference electrode. All the potentials were recorded with respect to SCE.

RESULTS AND DISCUSSION

Synthesis and Morphology of TiO_2-NSs Grown on CP Electrode. The morphologies of CPs and TiO_2-NSs/CPs were first characterized by FESEM and shown in Figure 1. CP was an intertexture consisting of carbon fibers with diameters of 6−8 μm, which formed a very rough surface (Figure 1a). After hydrothermal reaction, the CP surface was uniformly covered with a dense layer (Figure 1b) and its original topography maintained. A magnified FESEM image in Figure 1c shows that the dense layer was composed of vertically oriented nanosheets (NSs) with intervals on the top less than about 1 μm, which formed vertically penetrating pores through the layer. It is expected that such a 3D open porous structure is favorable for biofilm growth as well as permeability of electrolyte, organic substrates and electron mediators.[24] The lateral view of the cover layer indicates that the rectangular NSs were about 2 μm in length and 200−600 nm in width (Figure 1d) whereas the thickness of the NSs was about 15 nm (Figure S2, Supporting Information). From the intuitionistic observation, these NSs grew upward from surface of CP could construct direct pathways for delivering electrons from exoelectrogens in biofilm to CP substrate.

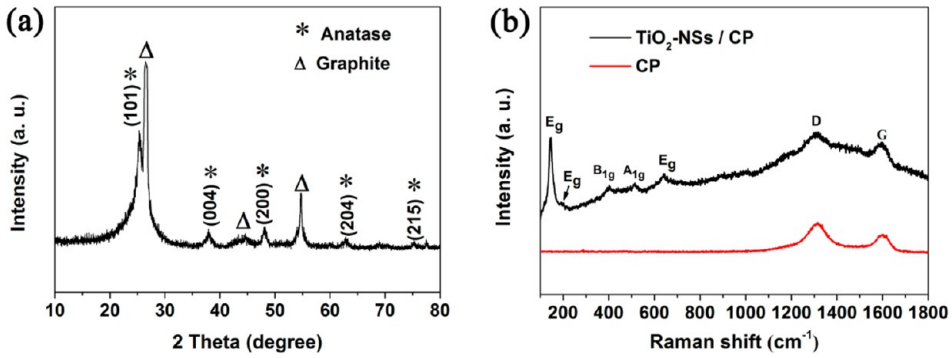

Figure 3. XRD pattern (a) and Raman spectra (b) of the TiO_2-NSs layer grown on the CP under optimal preparation conditions.

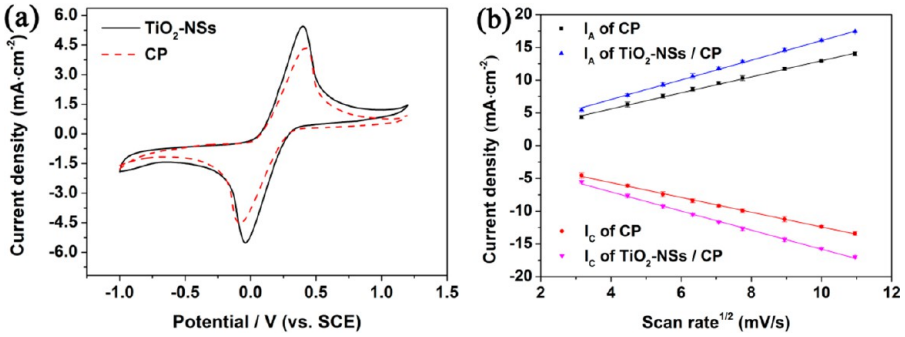

Figure 4. CV of TiO_2-NSs/CP and bare CP electrode in PBS containing 50 mM potassium ferricyanide at scan rate of 10 mV/s (a), and the linear fitting of redox peak current with square root of scanning rate for both electrodes (b).

To grow the NSs layer on the CP surface, a seed layer of anatase TiO_2 was first coated on CP by dipping the CP into a sol solution of colloidal TiO_2 and then drying. During hydrothermal treating, the deposited TiO_2 nanoparticles reacted with concentrated NaOH to form new crystals on CP surface through dissolution–nucleation–growth process at elevated temperature and pressure according to previous reports.[33] The product of hydrothermal reaction is closely related to its reaction parameters. Under current conditions, it was found that AC powders facilitated the formation of the NSs layer on the CP surface. Figure 2 shows the influence of AC powders on the morphology of the TiO_2 layer. Without addition of AC powders in the hydrothermal reaction solution, it always formed long and disordered nanowires on the CP surface (Figure 2a), although the nanowires uniformly covered the substrate (Figure S1, Supporting Information). In the presence of AC powders, NSs were formed gradually with the increasing amount of AC powders (Figure 2b,c). When addition of AC powders was over 150 mg, almost all the growing TiO_2 was in the shape of a nanosheet or nanobelt (Figure 2c,d). However, the best addition was 200 mg, which resulted in the formation of up-standing nanosheets (Figure 1c) instead of disorderly tilted nanosheets (Figure 2d). In the following experiment, all the samples were obtained under the addition of 200 mg of AC powders.

However, how AC powders play their role in the hydrothermal process is not well understood, and the detailed mechanism needs to be investigated in the future. It is well-known that diffusion field of reactive species around substrates affects recrystallization during the hydrothermal process. For example, when the precursor solution was stirred in the presence of a glass substrate, the rutile needles were deposited instead of the nanosheets.[34] Therefore, we speculate that one possible effect of AC powders may be controlling the concentration of species with the time in reaction solution through adsorption–desorption interaction.

Phase Identity of TiO_2-NSs. Upon addition of 200 mg of AC powders in an autoclave, a well oriented TiO_2-NSs layer could be observed throughout the substrate. It is worth mentioning that no part of the layer was shedding off from substrate when the modified CP was immersed in water or cultivation medium for as long as 2 months. This shows good contact between the CP and TiO_2-NSs, which is desired for MFC applications. To examine the crystal structure of the over layer, XRD and Raman spectra were obtained, as in Figure 3. In XRD spectra, apart from the peaks arising from CP substrate, other peaks at 2θ of 25.4, 37.8, 48.2, 62.8 and 75° can be indexed to pure anatase phase of TiO_2 (JCPDS card no. 21-1272) corresponding to diffractions from the (101), (004), (200), (204) and (215) planes, respectively. The diffraction peak from the (105) plane was overlapped with the diffraction from CP substrate at 2θ of about 54–55°.

Raman scattering is very sensitive to crystallinity and microstructures of materials.[35] The polymorphs of TiO_2-NSs/CP was further characterized by Raman spectroscopy. Two peaks at ~1308 and 1597 cm^{-1} were the D and G bands of carbon paper substrate due to disordered and graphitic phase, which also appeared in bare CP. The bands around 145 (E_g), 398 (B_{1g}), 514 (A_{1g}/B_{1g}), 641 cm^{-1} (E_g) and a weak shoulder near 196 cm^{-1} (E_g) matched well with vibrational modes of typical anatase and no peaks due to other TiO_2 phase were observed.[36] This clearly indicated that an anatase phase was formed in the nanosheets.

In short, XRD and Raman characterizations of TiO_2-NSs/CP consistently indicate formation of anatase TiO_2 crystals on the CP substrate, which occurred upon annealing the samples after

dx.doi.org/10.1021/am506360x | ACS Appl. Mater. Interfaces 2015, 7, 400–408

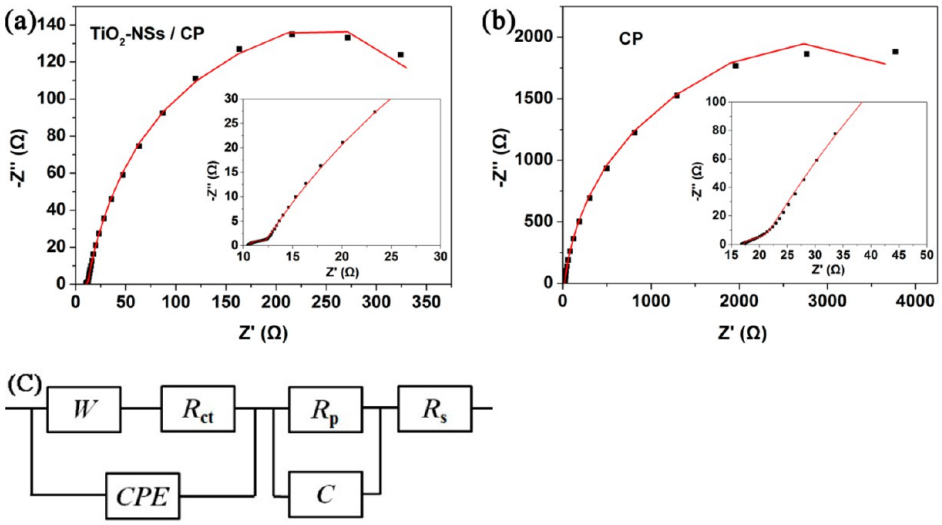

Figure 5. Nyquist plots of TiO_2-NSs/CP (a) and bare CP (b) electrodes with insets illustrating the spectra in middle to high frequency range, and an equivalent circuit for fitting Nyquist plots (c). The points in (a) and (b) represent experimental data while the line is fitting result, the χ^2 values of the fitting for TiO_2-NSs/CP and bare CP were 4.1×10^{-4} and 9.7×10^{-4}, respectively. The EIS was measured at an electrode potential of 0 V in PBS solution containing 50 mM potassium ferricyanide.

hydrothermal treating and washing with acid and water. This is similar to the report by Cortés-Jácome,[37] in which the anatase was produced during the transformation of titania nanotubes by in situ annealing at 550 °C in a nitrogen atmosphere.

Although the oriented TiO_2 nanosheets/flakesr were fabricated on substrates such as FTO/glass,[34,38,39] or a Ti plate,[40] relatively fewer examples of ordered TiO_2 nanosheets on C substrates were reported.[41,42] Here the upstanding TiO_2 nanosheets formed on a carbon based electrode.

Electrochemical Investigation of TiO_2-NSs/CP Electrode. To verify the interfacial electron transfer properties of the TiO_2-NSs/CP electrode, electrochemical experiment was conducted and compared with that of the CP electrode using $K_3[Fe(CN)_6]$ as a prober, which is often used in electrochemical systems to demonstrate the properties of relevant electrodes.[43] CV in Figure 4a exhibited quasi-reversible characterization generally accompanying in electrochemical process of redox couple $Fe(CN)_6^{3-}/Fe(CN)_6^{4-}$, i.e., approximate ratio of 1 for I_{pa}/I_{pc} independent of scan rates ν. In addition, the average value of redox peak potentials was 0.17 and 0.20 V on CP and TiO_2-NSs/CP electrodes respectively, which was close to the formal potential of $Fe(CN)_6^{3-}/Fe(CN)_6^{4-}$. The good linear relationship between peak current density I_A or I_C and square root of the scanning rate, $\nu^{1/2}$, was established in both electrodes (Figure 4b), which implied the electrochemical reaction was subject to a diffusion-controlled process. From Figure 4a, a bigger peak current was observed on the TiO_2-NSs/CP electrode. It is well-known that electrode reactions as heterogeneous processes can be markedly affected by the microstructure, roughness and function groups present on the electrode surface. Vertically oriented TiO_2-NSs obviously enlarged the surface area of the modified electrode upon formation of a 3D open porous interface, and this point can be verified by the larger tilt of the straight line represented for the TiO_2-NSs/CP electrode in Figure 4b. Normally, a larger surface area will lead to a larger electrochemically active surface area,[44] and then a larger current density, which is reflected in Figure 4a. However, quantitatively comparing the electrochemically active surface area of two electrodes from lines in Figure 4b according to the Randles−Sevcik equation would be improper due to the intrinsic differences of surface structure between CP and TiO_2-NSs/CP.

Besides the change of electrochemically active surface area, the surface modification may also modify interfacial mass transport kinetics and/or electron transfer kinetics of redox active species. To further explore the effects of the TiO_2-NSs layer on the electrode reactions, EIS analysis was carried out. The real part (Z_{re}) and imaginary part (Z_{im}) of the impedance are shown in Figure 5a,b. The Nyquist plot of TiO_2-NSs/CP exhibited a small and incomplete semicircle in high frequency region and a large arc in the low frequency region. A similar feature was also observed in the Nyquist plot of the CP electrode but with much larger diameters for the arc. An equivalent circuit in Figure 5c was used to fit measured data using ZView 3.0 software, where R_{ct} is the charge-transfer resistance and W is Warburg impedance corresponding to the diffusion resistance in working electrode, while a constant phase element (CPE) describes the diffusion double layer capacitance of a rough surface. R_p represents the charge-transfer resistance at the counter electrode/electrolyte interface and parallels with a capacitor C to account for the small semicircle in the high frequency region. The other resistance was represented by a series resistance R_s. A comparison of the fitting results of the TiO_2-NSs/CP electrode with the corresponding values of the bare CP electrode shows that R_{ct} (266.4 vs 2965 Ω) and diffusion resistance W-R (139 vs 2025 Ω) are both remarkably reduced, indicating a faster electron-transfer rate and facilitating mass transport process on the TiO_2-NSs/CP electrode. In addition, CPE-T, the capacitance of the diffusion layer, was significantly increased (2.98×10^{-3} vs 3.52×10^{-4} F/s^{1-P}) and the CPE-P, a parameter less than 1, estimating the inhomogeneity of an electrode surface, was decreased (0.81 vs 0.91), corresponding to enlarged surface area and roughness for TiO_2-NSs/CP electrode. The EIS results show that the TiO_2-NSs layer was beneficial to the interfacial electron transfer due to superior electron and mass transfer kinetics, which was in line with the CV results (Figure 4).

dx.doi.org/10.1021/am506360x | ACS Appl. Mater. Interfaces 2015, 7, 400−408

Performance of a Mixed Consortia Inoculated MFCs Using TiO_2-NSs/CP as Anode. Electrochemical investigation of the TiO_2-NSs/CP electrode suggests that the as prepared electrode has a larger electrochemical area as well as enhanced mass transport. We therefore expect that the modified electrode could produce enhanced current generation when used in MFCs, which would be highly desired considering the excellent biocompatibility and chemical stability of the TiO_2 layer. We examined the performance of mixed consortia inoculated MFCs using TiO_2-NSs/CP as the anode without compositing other conducting materials such as PANI or CNTs. Figure 6 shows power output and polarization curves of the MFCs using different anodes. As TiO_2-NSs/CP was used as the anode, a significant performance improvement was observed. The maximum output power density for the MFC equipped TiO_2-NSs/CP anode was 690 mW/m^3, corresponding to a 63% increase relative to that of 423 mW/m^3 for the MFC equipped bare CP anode. The total internal resistance R_{int} of the MFCs was estimated from the external resistance used to measure the point of maximum power density, to be 100 and 200 Ω, respectively, for the as-built MFC and control MFC, which were close to the values (109 and 213 Ω) obtained by linear fitting of voltage drops in the ohmic region of polarization curves (Figure S6, Supporting Information).[45] Obviously, different performance of the MFCs arose from the different anode and biofilm on it.

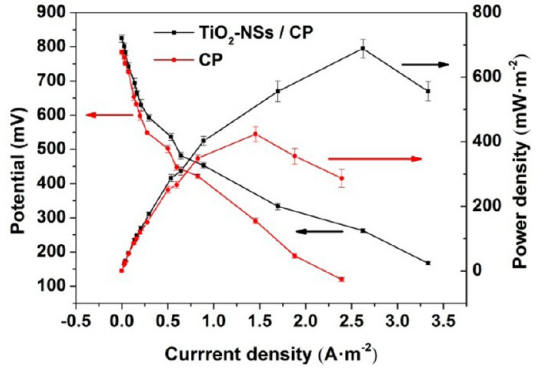

Figure 6. Power output and polarization curves of the MFCs equipped using different anodes.

EET in the Interface of TiO_2-NSs/CP Electrode. To best understand the performance of the MFCs, CV experiments were performed on the MFC using the anode as the working electrode and the cathode as the counter electrode to ascertain the biofilm-associated electron transfer process. As shown in Figure 7, more than one electrochemical processes occurred in the anode. One of the redox reactions possessed a midpoint potential E_m of about 0.20 V, which was close to cathodic potential (0.26 V). The oxidative peak current due to this reaction was dramatically dropped when the anolyte was replaced with fresh medium, indicating this peak possibly arose from the redox active metabolic intermediate secreted by biofilm. However, this redox process should make hardly any contribution to the power generation because of its relatively positive oxidative potential. Another redox reaction possessed a midpoint potential E_m from −0.2 to −0.23 V, which was in the range of formal potentials of various OMCs[16,46] found in exoelectrogens. It is known that the attached OMCs can mediate direct electron transfer from the cell surface to solid oxides or graphite electrode responsible for electricity generation in MFCs and also play the important roles in

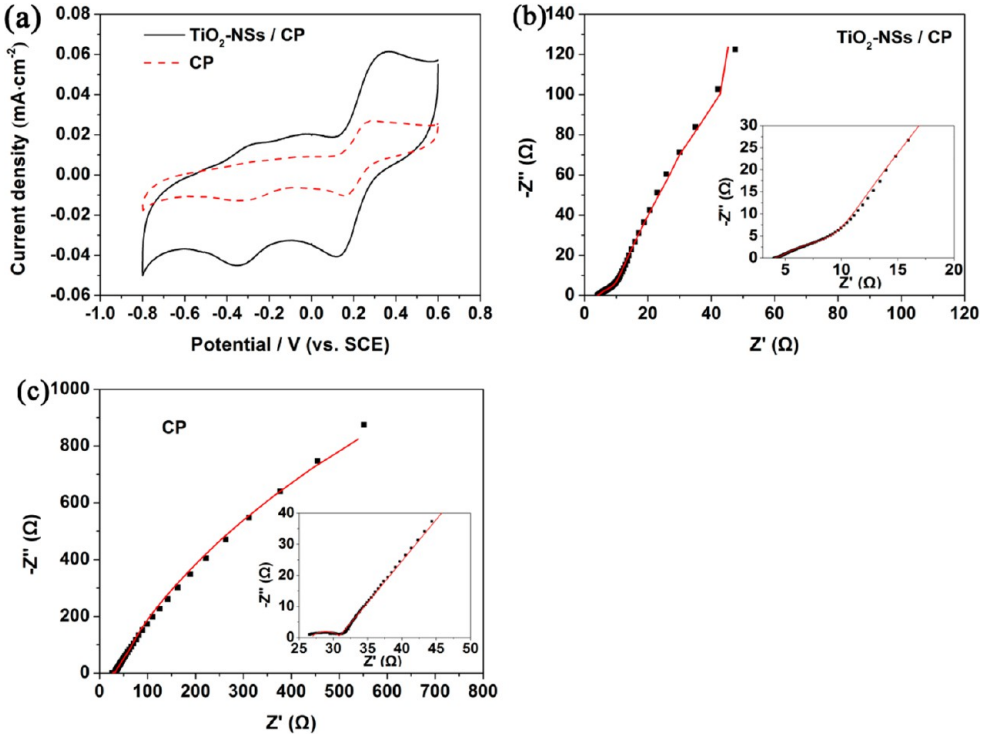

Figure 7. CV of the different anode biofilms (a), and EIS spectra of TiO_2-NSs/CP anode (b) as well as bare CP anode (c). The points in panels b and c represent experimental data whereas the line is the fitting result. The χ^2 values of the fitting for TiO_2-NSs/CP and bare CP were 4.6×10^{-4} and 2.2×10^{-3}, respectively. CV and EIS were measured in the MFCs with anode as working electrode. EIS was measured at −0.25 V.

dx.doi.org/10.1021/am506360x | ACS Appl. Mater. Interfaces 2015, 7, 400−408

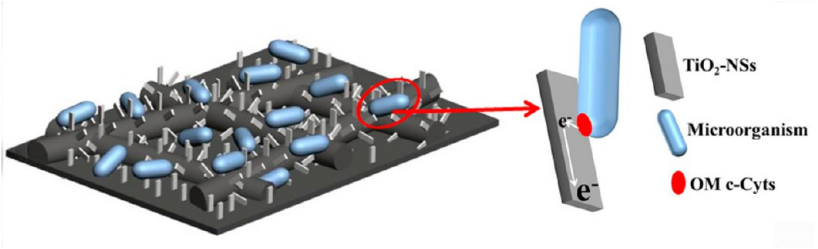

Figure 8. Schematic illustration of the formation of up growing TiO_2-NSs layer on CP electrode and bacterial EET on it.

microbial activities in anaerobic subsurface environments. Reasonably, the redox processes with E_m values from −0.2 to −0.23 V could be attributed to interfacial electron transfer between OMCs of bacteria and the electrode and account for the current generation. However, indirect electron transfer mechanisms, namely via electron mediators, could not be excluded from CV experiments. Because some electron mediators secreted by bacteria, such as quinone and phenazine-like compounds[47,48] have midpoint potentials near this region. So, the larger CV current density of the TiO_2-NSs/CP anode biofilm in Figure 7a was coincident with the enhanced power output, shown in Figure 6. Further insights into the anode electron transfer by these biofilms were gained through EIS measurement performed on the MFCs (Figure 7b-c). The fitting results showed that both the diffusion resistances W-R (3636 Ω) and electron transfer resistances R_{ct} (13.3 Ω) on the TiO_2-NSs/CP anode were decreased relative to the corresponding values of 4041 and 43.6 Ω on the bare CP electrode, again demonstrating the enhanced EET activity of biofilm due to the TiO_2-NSs layer.

According to the above discussion, a layer of vertically oriented TiO_2-NSs brings several advantages beneficial to the interfacial redox process, and promotes bacterial EET, as schematically illustrated in Figure 8. Briefly, the TiO_2-NSs on the CP surface formed a 3D open porous structure, which was a favorable electrode surface for MFCs. Previous research efforts have shown that a rough interface with porous structure in micro/submicrosizes is advantageous because this will enable extensive biofilm formation and efficient transport of nutrients and wastes.[49] Vertically oriented TiO_2-NSs provide not only a large "bioaccessible" surface area but also excellent biocompatibility for microbe growth, as seen from the dense biofilm on the modified electrode (Figure S7, Supporting Information). Furthermore, the vertically penetrating pores through the layer promote the mass transport, as evidenced by reduced diffusion resistance. A strengthened diffusion process is helpful to bacteria growth and indirect electron transfer via electron mediators produced by a biocatalyst. Previous studies have also demonstrated that it is easy to achieve direct electron transfer between TiO_2 and redox enzymes/proteins,[21] and nanostructured TiO_2 such as nanoneedles,[50] nanorods[51] and nanofiliforms[52] were utilized to enhance direct electrochemistry of an enzymatic electrode and hence the performance of biosensors/biocatalysts. TiO_2-NSs on a modified CP electrode provided a large contact area between the TiO_2 and the biofilm. The surface group on TiO_2 such as hydroxyl group can reinforce the adhesion of bacteria, and the microstructure of TiO_2 was also helpful for direct electron transfer from redox proteins to TiO_2.[53] Together with another brilliant feature of up-standing nanosheets, i.e., facilitating the movement of delivered electrons from OMCs to electrode just as previous observation on the transport of photoexited electrons along oriented TiO_2 nanostructures,[30] faster electron transfer on TiO_2-NSs/CP should be obtained, which was illustrated from the results of CV and EIS measurement. All these properties of modified electrode are anticipated to yield significant improvement of the MFC performance and account for the observed difference in Figure 6.

CONCLUSION

The surface of a CP electrode was successfully modified by a layer of vertically oriented TiO_2 nanosheets. The bioelectricity generation on such a modified CP electrode without any additional conductive materials was superior to that of a bare CP electrode. The unique surface structure of TiO_2-NSs/CP electrode plays a critical role in enhancing power output of MFCs. Vertically oriented TiO_2-NSs on a CP surface formed vertically penetrating pores that offer a large contact area to OMCs for direct electron transfer, high biocompatibility, facilitating molecular diffusion and favorable electron transport pathways. These results demonstrated the strategy of a properly tailored TiO_2 nanostructure on electrode surface to promote EET of exoelectrogens that could be applicable to other semiconductor materials, and provide a new pathway for performance improvement of bioanode and relevant MFCs. Due to the common usage of carbon based electrode, the results from current study may also find potential applications in other electrochemistry technologies such as electric catalysis and electroanalysis.

ASSOCIATED CONTENT

Supporting Information

FESEM images of modified CP surfaces obtained under different amount of added AC powders, XRD of CP, cyclic voltammograms of $K_3[Fe(CN)_6]$ at different scan rates, CV of the electrodes in cultivation medium solution, linear fitting of voltage drops in the ohmic region of polarization curve, FESEM images of microbes grown on electrode surface, and MFC operation in long-term. This material is available free of charge via the Internet at http://pubs.acs.org.

AUTHOR INFORMATION

Corresponding Author

*D. Fu. E-mail: fudegang@seu.edu.cn.

Notes

The authors declare no competing financial interest.

ACKNOWLEDGMENTS

This work was supported by National Natural Science Foundation of China (No. 51172043), and the State Key Laboratory of Bioelectronics, Southeast University. The authors thank Xiuqin Jia for assistance on drawing of Figure 8.

REFERENCES

(1) Marsili, E.; Rollefson, J. B.; Baron, D. B.; Hozalski, R. M.; Bond, D. R. Microbial Biofilm Voltammetry: Direct Electrochemical Characterization of Catalytic Electrode-Attached Biofilms. *Appl. Environ. Microbiol.* **2008**, *74*, 7329−37.

(2) Liu, H. A.; Matsuda, S.; Kato, S.; Hashimoto, K.; Nakanishi, S. Redox-Responsive Switching in Bacterial Respiratory Pathways Involving Extracellular Electron Transfer. *ChemSusChem* **2010**, *3*, 1253−1256.

(3) Okamoto, A.; Nakamura, R.; Hashimoto, K. In-Vivo Identification of Direct Electron Transfer from *Shewanella oneidensis* MR-1 to Electrodes Via Outer-Membrane OmcA-MtrCAB Protein Complexes. *Electrochim. Acta* **2011**, *56*, 5526−5531.

(4) Yong, Y. C.; Yu, Y. Y.; Yang, Y.; Liu, J.; Wang, J. Y.; Song, H. Enhancement of Extracellular Electron Transfer and Bioelectricity Output by Synthetic Porin. *Biotechnol. Bioeng.* **2013**, *110*, 408−416.

(5) Yong, Y. C.; Yu, Y. Y.; Li, C. M.; Zhong, J. J.; Song, H. Bioelectricity Enhancement Via Overexpression of Quorum Sensing System in Pseudomonas Aeruginosa-Inoculated Microbial Fuel Cells. *Biosens. Bioelectron.* **2011**, *30*, 87−92.

(6) Szczupak, A.; Kol-Kalmanz, D.; Alfonta, L. A Hybrid Biocathode: Surface Display of O_2-Reducing Enzymes for Microbial Fuel Cell Applications. *Chem. Commun.* **2012**, *48*, 49−51.

(7) Kumar, G. G.; Sarathi, V. G. S.; Nahm, K. S. Recent Advances and Challenges in the Anode Architecture and Their Modifications for the Applications of Microbial Fuel Cells. *Biosens. Bioelectron.* **2013**, *43*, 461−475.

(8) Manickam, S. S.; Karra, U.; Huang, L. W.; Bui, N. N.; Li, B. K.; McCutcheon, J. R. Activated Carbon Nanofiber Anodes for Microbial Fuel Cells. *Carbon* **2013**, *53*, 19−28.

(9) Logan, B. E.; Hamelers, B.; Rozendal, R. A.; Schrorder, U.; Keller, J.; Freguia, S.; Aelterman, P.; Verstraete, W.; Rabaey, K. Microbial Fuel Cells: Methodology and Technology. *Environ. Sci. Technol.* **2006**, *40*, 5181−5192.

(10) Tang, X. H.; Guo, K.; Li, H. R.; Du, Z. W.; Tian, J. L. Electrochemical Treatment of Graphite to Enhance Electron Transfer from Bacteria to Electrodes. *Bioresour. Technol.* **2011**, *102*, 3558−3560.

(11) Liu, Y.; Du, Y.; Li, C. M. Direct Electrochemistry based Biosensors and Biofuel Cells Enabled with Nanostructured Materials. *Electroanalysis* **2013**, *25*, 815−831.

(12) Greiner, M. T.; Lu, Z. H. Thin-Film Metal Oxides in Organic Semiconductor Devices: Their Electronic Structures, Work Functions and Interfaces. *NPG Asia Mater.* **2013**, *5*, 16.

(13) Singh, K.; Nowotny, J.; Thangadurai, V. Amphoteric Oxide Semiconductors for Energy Conversion Devices: A Tutorial Review. *Chem. Soc. Rev.* **2013**, *42*, 1961−1972.

(14) Lv, Z. S.; Xie, D. H.; Yue, X. J.; Feng, C. H.; Wei, C. H. Ruthenium Oxide-Coated Carbon Felt Electrode: A Highly Active Anode for Microbial Fuel Cell Applications. *J. Power Sources* **2012**, *210*, 26−31.

(15) Lower, S. K.; Hochella, M. F.; Beveridge, T. J. Bacterial Recognition of Mineral Surfaces: Nanoscale Interactions between *Shewanella* and α-FeOOH. *Science* **2001**, *292*, 1360−1363.

(16) Nakamura, R.; Ishii, K.; Hashimoto, K. Electronic Absorption Spectra and Redox Properties of C Type Cytochromes in Living Microbes. *Angew. Chem., Int. Ed.* **2009**, *48*, 1606−1608.

(17) Peng, X. H.; Yu, H. B.; Wang, X.; Gao, N. S. J.; Geng, L. J.; Ai, L. N. Enhanced Anode Performance of Microbial Fuel Cells by Adding Nanosemiconductor Goethite. *J. Power Sources* **2013**, *223*, 94−99.

(18) Lu, A. H.; Li, Y.; Jin, S.; Wang, X.; Wu, X. L.; Zeng, C. P.; Li, Y.; Ding, H. R.; Hao, R. X.; Lv, M.; Wang, C. Q.; Tang, Y. Q.; Dong, H. L. Growth of Non-Phototrophic Microorganisms Using Solar Energy through Mineral Photocatalysis. *Nat. Commun.* **2012**, *3*, 8.

(19) Que, L. F.; Lan, Z.; Wu, W. X.; Wu, J. H.; Lin, J. M.; Huang, M. L. High-Efficiency Dye-Sensitized Solar Cells Based on Ultra-Long Single Crystalline Titanium Dioxide Nanowires. *J. Power Sources* **2014**, *266*, 440−447.

(20) Jin, Z.; Meng, F. L.; Jia, Y.; Luo, T.; Liu, J. Y.; Sun, B.; Wang, J.; Liu, J. H.; Huang, X. J. Porous TiO_2 Nanowires Derived from Nanotubes: Synthesis, Characterzation and Their Enhanced Photocatalytic Properties. *Microporous Mesoporous Mater.* **2013**, *181*, 146−153.

(21) Bao, S. J.; Li, C. M.; Zang, J. F.; Cui, X. Q.; Qiao, Y.; Guo, J. New Nanostructured Tio_2 for Direct Electrochemistry and Glucose Sensor Applications. *Adv. Funct. Mater.* **2008**, *18*, 591−599.

(22) Salari, M.; Aboutalebi, S. H.; Konstantinov, K.; Liu, H. K. A Highly Ordered Titania Nanotube Array as a Supercapacitor Electrode. *Phys. Chem. Chem. Phys.* **2011**, *13*, 5038−5041.

(23) Zhou, H.; Liu, L.; Yin, K.; Liu, S. L.; Li, G. X. Electrochemical Investigation on the Catalytic Ability of Tyrosinase with the Effect of Nano Titanium Dioxide. *Electrochem. Commun.* **2006**, *8*, 1168−1172.

(24) Qiao, Y.; Bao, S. J.; Li, C. M.; Cui, X. Q.; Lu, Z. S.; Guo, J. Nanostructured Polyanifine/Titanium Dioxide Composite Anode for Microbial Fuel Cells. *ACS Nano* **2008**, *2*, 113−119.

(25) Wen, Z. H.; Ci, S. Q.; Mao, S.; Cui, S. M.; Lu, G. H.; Yu, K. H.; Luo, S. L.; He, Z.; Chen, J. H. TiO_2 Nanoparticles-Decorated Carbon Nanotubes for Significantly Improved Bioelectricity Generation in Microbial Fuel Cells. *J. Power Sources* **2013**, *234*, 100−106.

(26) Leelavathi, A.; Madras, G.; Ravishankar, N. Origin of Enhanced Photocatalytic Activity and Photoconduction in High Aspect Ratio Zno Nanorods. *Phys. Chem. Chem. Phys.* **2013**, *15*, 10795−10802.

(27) Talapin, D. V.; Lee, J. S.; Kovalenko, M. V.; Shevchenko, E. V. Prospects of Colloidal Nanocrystals for Electronic and Optoelectronic Applications. *Chem. Rev.* **2010**, *110*, 389−458.

(28) Tisdale, W. A.; Williams, K. J.; Timp, B. A.; Norris, D. J.; Aydil, E. S.; Zhu, X. Y. Hot-Electron Transfer from Semiconductor Nanocrystals. *Science* **2010**, *328*, 1543−1547.

(29) Wu, D. P.; Wang, Y.; Dong, H.; Zhu, F.; Gao, S. Y.; Jiang, K.; Fu, L. M.; Zhang, J. P.; Xu, D. S. Hierarchical TiO_2 Microspheres Comprised of Anatase Nanospindles for Improved Electron Transport in Dye-Sensitized Solar Cells. *Nanoscale* **2013**, *5*, 324−330.

(30) Macaira, J.; Andrade, L.; Mendes, A. Review on Nanostructured Photoelectrodes for Next Generation Dye-Sensitized Solar Cells. *Renewable Sustainable Energy Rev.* **2013**, *27*, 334−349.

(31) Galkina, O. L.; Sycheva, A.; Blagodatskiy, A.; Kaptay, G.; Katanaev, V. L.; Seisenbaeva, G. A.; Kessler, V. G.; Agafonov, A. V. The Sol-Gel Synthesis of Cotton/TiO_2 Composites and Their Antibacterial Properties. *Surf. Coat. Technol.* **2014**, *253*, 171−179.

(32) Cao, X. X.; Huang, X.; Liang, P.; Boon, N.; Fan, M. Z.; Zhang, L.; Zhang, X. Y. A Completely Anoxic Microbial Fuel Cell Using a Photo-Biocathode for Cathodic Carbon Dioxide Reduction. *Energy Environ. Sci.* **2009**, *2*, 498−501.

(33) Kiatkittipong, K.; Ye, C. H.; Scott, J.; Amal, R. Understanding Hydrothermal Titanate Nanoribbon Formation. *Cryst. Growth Des.* **2010**, *10*, 3618−3625.

(34) Aoyama, Y.; Oaki, Y.; Ise, R.; Imai, H. Mesocrystal Nanosheet of Rutile TiO_2 and Its Reaction Selectivity as a Photocatalyst. *CrystEngComm* **2012**, *14*, 1405−1411.

(35) Ma, R. Z.; Fukuda, K.; Sasaki, T.; Osada, M.; Bando, Y. Structural Features of Titanate Nanotubes/Nanobelts Revealed by Raman, X-Ray Absorption Fine Structure and Electron Diffraction Characterizations. *J. Phys. Chem. B* **2005**, *109*, 6210−6214.

(36) Inoue, F.; Ando, R. A.; Corio, P. Raman Evidence of the Interaction between Multiwalled Carbon Nanotubes and Nanostructured TiO_2. *J. Raman Spectrosc.* **2011**, *42*, 1379−1383.

(37) Cortes-Jacome, M. A.; Ferrat-Torres, G.; Ortiz, L. F. F.; Angeles-Chavez, C.; Lopez-Salinas, E.; Escobar, J.; Mosqueira, M. L.; Toledo-Antonio, J. A. In Situ Thermo-Raman Study of Titanium Oxide Nanotubes. *Catal. Today* **2007**, *126*, 248−255.

(38) Gan, X. Y.; Gao, X. D.; Qiu, J. J.; He, P.; Li, X. M.; Xiao, X. D. TiO_2 Nanorod-Derived Synthesis of Upstanding Hexagonal Kassite Nanosheet Arrays: An Intermediate Route to Novel Nanoporous TiO_2 Nanosheet Arrays. *Cryst. Growth Des.* **2012**, *12*, 289−296.

(39) Feng, S. L.; Yang, J. Y.; Zhu, H.; Liu, M.; Zhang, J. S.; Wu, J.; Wan, J. Y. Synthesis of Single Crystalline Anatase TiO_2(001) Tetragonal Nanosheet-Array Films on Fluorine-Doped Tin Oxide Substrate. *J. Am. Ceram. Soc.* **2011**, *94*, 310−315.

(40) Hosono, E.; Matsuda, H.; Honma, I.; Ichihara, M.; Zhou, H. Synthesis of a Perpendicular TiO_2 Nanosheet Film with the Superhydrophilic Property without UV Irradiation. *Langmuir* **2007**, *23*, 7447−7450.
(41) Chen, C. J.; Hu, X. L.; Wang, Z. H.; Xiong, X. Q.; Hu, P.; Liu, Y.; Huang, Y. H. Controllable Growth of Tio_2-B Nanosheet Arrays on Carbon Nanotubes as a High-Rate Anode Material for Lithium-Ion Batteries. *Carbon* **2014**, *69*, 302−310.
(42) Guo, W. X.; Zhang, F.; Lin, C. J.; Wang, Z. L. Direct Growth of TiO_2 Nanosheet Arrays on Carbon Fibers for Highly Efficient Photocatalytic Degradation of Methyl Orange. *Adv. Mater.* **2012**, *24*, 4761−4764.
(43) Zhao, F.; Slade, R. C. T.; Varcoe, J. R. Techniques for the Study and Development of Microbial Fuel Cells: An Electrochemical Perspective. *Chem. Soc. Rev.* **2009**, *38*, 1926−1939.
(44) Tremblay, M. L.; Martin, M. H.; Lebouin, C.; Lasia, A.; Guay, D. Determination of the Real Surface Area of Powdered Materials in Cavity Microelectrodes by Electrochemical Impedance Spectroscopy. *Electrochim. Acta* **2010**, *55*, 6283−6291.
(45) Fan, Y. Z.; Sharbrough, E.; Liu, H. Quantification of the Internal Resistance Distribution of Microbial Fuel Cells. *Environ. Sci. Technol.* **2008**, *42*, 8101−8107.
(46) Liu, H. A.; Newton, G. J.; Nakamura, R.; Hashimoto, K.; Nakanishi, S. Electrochemical Characterization of a Single Electricity-Producing Bacterial Cell of *Shewanella* by Using Optical Tweezers. *Angew. Chem., Int. Ed.* **2010**, *49*, 6596−6599.
(47) Yang, Y. G.; Xu, M. Y.; Guo, J.; Sun, G. P. Bacterial Extracellular Electron Transfer in Bioelectrochemical Systems. *Process Biochem.* **2012**, *47*, 1707−1714.
(48) Watanabe, K.; Manefield, M.; Lee, M.; Kouzuma, A. Electron Shuttles in Biotechnology. *Curr. Opin. Biotechnol.* **2009**, *20*, 633−41.
(49) He, Z. M.; Liu, J.; Qiao, Y.; Li, C. M.; Tan, T. T. Y. Architecture Engineering of Hierarchically Porous Chitosan/Vacuum-Stripped Graphene Scaffold as Bioanode for High Performance Microbial Fuel Cell. *Nano Lett.* **2012**, *12*, 4738−4741.
(50) Luo, Y. P.; Liu, H. Q.; Rui, Q.; Tian, Y. Detection of Extracellular H_2O_2 Released from Human Liver Cancer Cells Based on TiO_2 Nanoneedles with Enhanced Electron Transfer of Cytochrome C. *Anal. Chem.* **2009**, *81*, 3035−3041.
(51) Yang, Z. J.; Tang, Y.; Li, J.; Zhang, Y. C.; Hu, X. Y. Facile Synthesis of Tetragonal Columnar-Shaped TiO_2 Nanorods for the Construction of Sensitive Electrochemical Glucose Biosensor. *Biosens. Bioelectron.* **2014**, *54*, 528−533.
(52) Lee, S. Y.; Matsuno, R.; Ishihara, K.; Takai, M. Direct Electron Transfer with Enzymes on Nanofiliform Titanium Oxide Films with Electron-Transport Ability. *Biosens. Bioelectron.* **2013**, *41*, 289−293.
(53) Li, Q.; Cheng, K.; Weng, W. J.; Du, P. Y.; Han, G. R. Highly Sensitive Hydrogen Peroxide Biosensors Based on TiO_2 Nanodots/ITO Electrodes. *J. Mater. Chem.* **2012**, *22*, 9019−9026.